Eur. Phys. J. C (2020) 80:22
https://doi.org/10.1140/epjc/s10052-019-7568-8

THE EUROPEAN PHYSICAL JOURNAL C

Regular Article - Theoretical Physics

Ξ_c and Ξ_b excited states within a $SU(6)_{lsf} \times$ HQSS model

J. Nieves[1], **R. Pavao**[1], **L. Tolos**[2,3,4,5,a]

[1] Instituto de Física Corpuscular (centro mixto CSIC-UV), Institutos de Investigación de Paterna, Aptdo. 22085, 46071 Valencia, Spain
[2] Institut für Theoretische Physik, University of Frankfurt, Max-von-Laue-Str. 1, 60438 Frankfurt am Main, Germany
[3] Frankfurt Institute for Advanced Studies, University of Frankfurt, Ruth-Moufang-Str. 1, 60438 Frankfurt am Main, Germany
[4] Institute of Space Sciences (ICE, CSIC), Campus UAB, Carrer de Can Magrans, 08193 Barcelona, Spain
[5] Institut d' Estudis Espacials de Catalunya (IEEC), 08034 Barcelona, Spain

Received: 14 November 2019 / Accepted: 14 December 2019

Abstract We study odd parity $J = 1/2$ and $J = 3/2$ Ξ_c resonances using a unitarized coupled-channel framework based on a $SU(6)_{lsf} \times$HQSS-extended Weinberg–Tomozawa baryon–meson interaction, while paying a special attention to the renormalization procedure. We predict a large molecular $\Lambda_c \bar{K}$ component for the $\Xi_c(2790)$ with a dominant 0^- light-degree-of-freedom spin configuration. We discuss the differences between the $3/2^-$ $\Lambda_c(2625)$ and $\Xi_c(2815)$ states, and conclude that they cannot be SU(3) siblings, whereas we predict the existence of other Ξ_c-states, one of them related to the two-pole structure of the $\Lambda_c(2595)$. It is of particular interest a pair of $J = 1/2$ and $J = 3/2$ poles, which form a HQSS doublet and that we tentatively assign to the $\Xi_c(2930)$ and $\Xi_c(2970)$, respectively. Within this picture, the $\Xi_c(2930)$ would be part of a SU(3) sextet, containing either the $\Omega_c(3090)$ or the $\Omega_c(3119)$, and that would be completed by the $\Sigma_c(2800)$. Moreover, we identify a $J = 1/2$ sextet with the $\Xi_b(6227)$ state and the recently discovered $\Sigma_b(6097)$. Assuming the *equal spacing rule* and to complete this multiplet, we predict the existence of a $J = 1/2$ Ω_b odd parity state, with a mass of 6360 MeV and that should be seen in the $\Xi_b \bar{K}$ channel.

1 Introduction

The study of heavy baryons with charm or bottom content has been the subject of much interest over the past years in view of newly discovered states [1]. In particular, there has been a tremendous effort to understand the nature of the experimental states within conventional quarks models, QCD sum-rules frameworks, QCD lattice analysis or molecular baryon–meson models (see Refs. [2–7] for recent reviews).

The attention has been recently revived by the experimental observation of several excited states. Recent detections have been reported by the LHCb Collaboration regarding five Ω_c excited states in the $\Xi_c^+ K^-$ spectrum in pp collisions [8], and the excited $\Xi_b(6227)$ state in $\Lambda_b^0 K^-$ and $\Xi_b^0 \pi^-$ invariant mass spectra also in pp collisions [9]. Moreover, the Belle Collaboration has confirmed the observation of four of the excited Ω_c states [10], and detected the $\Xi_c(2930)$ state in its decay to $\Lambda_c^+ K^-$ in $B^- \to K^- \Lambda_c^+ \bar{\Lambda}_c^-$ decays [11].

In view of these new observations, a large theoretical activity has been indeed triggered, in particular within dynamical approaches based on a molecular description of these states. Starting from the newly observed Ω_c states, the molecular models of Refs. [12,13] have been reanalyzed in view of the new discoveries. While in Ref. [14] two Ω_c resonant states at 3050 MeV and 3090 MeV with $J^P = 1/2^-$ were obtained, being identified with two of the experimental states, in Ref. [15] two $J^P = 1/2^-$ Ω_c states and one $J^P = 3/2^-$ Ω_c were determined within an extended local hidden gauge approach, the first two in good agreement with [14]. Other theoretical works also examined the Ω_c sector, trying to explain the extra broad structure observed by the LHCb around 3188 MeV [8]. In Ref. [16] it was shown that this bump could be interpreted as the superposition of two $D\Xi$ bound states, whereas in Ref. [17] a loosely bound molecule of mass 3140 MeV was determined.

With regards to Ξ_c, the theoretical analysis based on the local hidden gauge formalism has shown that not only the $\Xi_c(2930)$ can have a molecular interpretation, but also other Ξ_c states around 3 GeV reported in the PDG [1]. In particular, the $\Xi_c(2790)$ would be a $J^P = 1/2^-$ molecular state, whereas $\Xi_c(2930)$, $\Xi_c(2970)$, $\Xi_c(3055)$ and $\Xi_c(3080)$ could be described as molecules with either $1/2^-$ or $3/2^-$ [18]. On the other hand, the same model has produced two states for $\Xi_b(6227)$ with masses close to the experimental one with similar widths, being the spin–parity assignment

[a] e-mail: tolos@ice.csic.es

Published online: 11 January 2020

Table 1 Excited Ξ_c states below 3 GeV and the excited Ξ_b state found experimentally [1]. We show the assigned J^P (when possible), the mass M and width Γ, as well as the decay channels

Baryon	J^P	$M\ (MeV)$	Γ (MeV)	Decay channels
$\Xi_c(2790)^+/\Xi_c(2790)^0$	$1/2^-$	$2792.4 \pm 0.5/2794.1 \pm 0.5$	$8.9 \pm 1.0/10.0 \pm 1.1$	$\Xi_c'\pi$
$\Xi_c(2815)^+/\Xi_c(2815)^0$	$3/2^-$	$2816.73 \pm 0.21/2820.26 \pm 0.27$	$2.43 \pm 0.26/2.54 \pm 0.25$	$\Xi_c'\pi$, $\Xi_c^*\pi$
$\Xi_c(2930)^+/\Xi_c(2930)^0$	?	$2942 \pm 5/2929.7^{+2.8}_{-5.0}$	$15 \pm 9/26 \pm 8$	$\Lambda_c^+K^-$, $\Lambda_c^+K_S^0$
$\Xi_c(2970)^+/\Xi_c(2970)^0$	?	$2969.4 \pm 0.8/2967.8^{+0.9}_{-0.7}$	$20.9^{+2.4}_{-3.5}/28.1^{+3.4}_{-4.0}$	$\Lambda_c^+\bar{K}\pi$, $\Sigma_c\bar{K}$, $\Xi_c 2\pi$, $\Xi_c'\pi$, $\Xi_c^*\pi$
$\Xi_b(6227)$	?	6226.9 ± 2	18 ± 6	$\Lambda_b^0K^-$, $\Xi_b^0\pi^-$

either $1/2^-$ or $3/2^-$ [18]. The Ξ_b state has been also studied within a unitarized model that uses the leading-order chiral Lagrangian in Refs. [19,20], identifying the $\Xi_b(6227)$ state as a S-wave $\Sigma_b\bar{K}$ molecule, with a preferred $1/2^-$ spin–parity assignment [20].

Over the past years, a unitarized coupled-channel scheme has been developed in Refs. [21–27] that implements heavy-quark spin symmetry (HQSS), which is a proper QCD symmetry that appears when the quark masses, such as that of the charm or bottom quark, become larger than the typical confinement scale. This approach is based on a consistent $\mathrm{SU}(6)_{\mathrm{lsf}} \times$ HQSS extension of the Weinberg–Tomozawa (WT) πN interaction, where "lsf" stands for light quark–spin–flavor symmetry, respectively. Within this framework, it has been identified a two-pole pattern for the $\Lambda_c(2595)$ resonance[1] [21,23], similar to the $\Lambda(1405)$ [29–31]. The same scheme has also generated dynamically the $\Lambda_b(5912)$ and $\Lambda_b(5920)$ narrow resonances, discovered by LHCb [32], which turn out to be HQSS partners, naturally explaining their approximate mass degeneracy [24].

More recently, the work of Ref. [23] has been revisited in view of the newly discovered Ω_c states, paying a special attention to the renormalization procedure used in the unitarized coupled-channel model and its impact on the Ω_c sector. In Ref. [33] it was shown that some (probably at least three) of the Ω_c states experimentally observed by LHCb would have $1/2^-$ or $3/2^-$.

The discovery of the $\Xi_c(2930)$ and $\Xi_b(6227)$ has stimulated and motivated further research along this line. In the present work we follow a similar procedure as described in [33] and study the possible molecular interpretation of those states, revisiting the previous works on the Ξ_c [23] and Ξ_b [24] sectors. However, in the Ξ_c sector we do not restrict ourselves to the recent $\Xi_c(2930)$ observation, but analyze all excited Ξ_c states found experimentally with masses up to 3 GeV [1]. The four excited Ξ_c states with masses below 3 GeV and the $\Xi_b(6227)$ are collected in Table 1, showing the assigned spin–parity J^P (when possible) as well as masses, widths, and decay channels. In this work we pay a special attention to the dependence on the renormalization scheme as well as to the flavor-symmetry content of the $\mathrm{SU}(6)_{\mathrm{lsf}} \times$ HQSS model, as we determine the possible HQSS partners and siblings among the experimental states while predicting new ones. Thus, we follow the discussion of Ref. [23] on its spin–flavor symmetry breaking pattern. Flavor SU(4) is not a good symmetry in the limit of a heavy charm quark, for this reason, instead of the breaking pattern $\mathrm{SU}(8) \supset \mathrm{SU}(4)$, we consider the pattern $\mathrm{SU}(8) \supset \mathrm{SU}(6)$, since the light spin–flavor group [SU(6)] is decoupled from heavy-quark spin transformations. This allows us to implement HQSS in the analysis and to unambiguously identify the corresponding multiplets among the resonances generated dynamically. At the same time, we are also able to assign approximate heavy [SU(8)] and light [SU(6)] spin–flavor multiplet labels to the states.

This work is organized as follows. In Sect. 2 we present the $\mathrm{SU}(6)_{\mathrm{lsf}} \times$ HQSS extension of the WT interaction, while in Sect. 3 we show our results for the Ξ_c and Ξ_b states,[2] respectively, and the possible experimental identification. Finally, in Sect. 4 we present our conclusions, emphasizing the possible classification of these experimental states according to the flavor-symmetry content of the scheme, while predicting new observations.

2 Formalism

We consider the sector with charm $C = 1$, strangeness $S = -1$ and isospin $I = 1/2$ quantum numbers, where the $\Xi_c(2930)$ state has been observed by the Belle Collaboration [11]. Also, we examine the bottom $B = -1$, strangeness $S = -1$ and isospin $I = 1/2$, where the $\Xi_b(6227)$ has been found [9]. In order to do so, we revise the results in Ref. [23] for the Ξ_c states and in Ref. [24] for Ξ_b ones.

[1] The details of this double pole structure, generated by the $\Sigma_c\pi$, ND and ND^* coupled-channels dynamics, depend strongly on the adopted renormalization scheme, which could considerably enhance the role played by the two latter channels around the resonance energy. This is discuss in detail in Ref. [28].

[2] From now on we refer to excited Ξ_c and Ξ_b independently of $1/2^-$ or $3/2^-$ spin–parity assignment.

In the case of the $C = 1$, $S = -1$ and $I = 1/2$ sector, the building-blocks are the pseudoscalar (D_s, D, K, π, η, $\bar{K}$) and vector (D_s^*, D^*, K^*, ρ, ω, $\bar{K}^*$, ϕ) mesons, and the spin-1/2 (Λ, Σ, Ξ, Λ_c, Σ_c, Ξ_c, Ξ_c', Ω_c), and spin-3/2 (Σ_c^*, Ξ_c^*, Ω_c^*) charmed baryons [21,23]. For the bottom sector $B = -1$, $S = -1$ and $I = 1/2$, one can substitute the c quark by a b quark, and we have the pseudoscalar ($\bar{B}_s$, $\bar{B}$, K, π, η, $\bar{K}$) and vector ($\bar{B}_s^*$, $\bar{B}^*$, K^*, ρ, ω, $\bar{K}^*$, ϕ) mesons, and the spin-1/2 (Λ, Σ, Ξ, Λ_b, Σ_b, Ξ_b, Ξ_b', Ω_b), and spin-3/2 (Σ_b^*, Ξ_b^*, Ω_b^*) baryons [24]. All baryon–meson pairs with ($C = 1/B = -1$, $S = -1$, $I = 1/2$) quantum numbers span the coupled-channel space for a given total angular momentum (J).

The S-wave tree level amplitudes between two baryon–meson channels are given by the $\mathrm{SU}(6)_{\mathrm{lsf}} \times$HQSS WT kernel,

$$V_{ij}^J(s) = D_{ij}^J \frac{2\sqrt{s} - M_i - M_j}{4 f_i f_j} \sqrt{\frac{E_i + M_i}{2M_i}} \sqrt{\frac{E_j + M_j}{2M_j}}. \quad (1)$$

The M_i and m_i are the masses of the baryon and meson in the i channel, respectively, and E_i is the center-of-mass energy of the baryon in the same channel,

$$E_i = \frac{s - m_i^2 + M_i^2}{2\sqrt{s}}. \quad (2)$$

The projection onto definite J is done as explained in Refs. [23,34,35]. In [34], only $J = 1/2$ baryons and pseudoscalar mesons are considered. The inclusion of spin $J = 3/2$ baryons and vector mesons was discussed in Appendix A of Ref. [23], using results derived in [35]. The hadron masses, meson decay constants, f_i, and D_{ij}^J matrices are taken from Refs. [23,24], where the underlying $\mathrm{SU}(6)_{\mathrm{lsf}} \times$ HQSS group structure of the interaction has been considered.

Starting from V_{ij}^J, we solve the Bethe–Salpeter equation (BSE) in coupled channels,

$$T^J(s) = \frac{1}{1 - V^J(s) G^J(s)} V^J(s), \quad (3)$$

where the $G^J(s)$ is a diagonal matrix that contains the different baryon–meson loop functions G_i,

$$G_i(s) = i 2 M_i \int \frac{d^4q}{(2\pi)^4} \frac{1}{q^2 - m_i^2 + i\epsilon} \frac{1}{(P-q)^2 - M_i^2 + i\epsilon}, \quad (4)$$

with P the total momentum of the system such that $P^2 = s$. We omit the index J from here on for simplicity. The bare loop function is logarithmically ultraviolet (UV) divergent and needs to be renormalized. This can be done by separating the divergent and finite parts of the loop function,

$$G_i(s) = \overline{G}_i(s) + G_i(s_{i+}), \quad (5)$$

with the finite part of the loop function, $\overline{G}_i(s)$, given in Refs. [33,34]. The divergent contribution of the loop function, $G_i(s_{i+})$ in Eq. (5) needs to be renormalized.

On the one hand, this can be done by one subtraction at certain scale ($\sqrt{s} = \mu$)

$$G_i^\mu(s) = \overline{G}_i(s) - \overline{G}_i(\mu^2), \quad (6)$$

where $\mu = \sqrt{m_{th}^2 + M_{th}^2}$, with m_{th} and M_{th} the masses of the meson and the baryon, respectively, that belong to the channel with the smallest threshold for a given (C, S, I) or (B, S, I) sectors. This common scale μ is chosen to be independent of total angular momentum J [13,36], and it is the approach used in the previous works of Refs. [23,24].

On the other hand, as discussed in our recent paper [33], we could also use a sharp-cutoff regulator Λ in momentum space, so that

$$G_i^\Lambda(s) = \overline{G}_i(s) + G_i^\Lambda(s_{i+}), \quad (7)$$

where $G_i^\Lambda(s_{i+})$ is given in Refs. [33,37].

Note that if one uses channel-dependent cutoffs, the one-subtraction renormalization scheme is recovered by choosing Λ_i in each channel in such a way that

$$G_i^{\Lambda_i}(s_{i+}) = -\overline{G}_i(\mu^2). \quad (8)$$

However, we employ a common UV cutoff for all baryon–meson loops within reasonable limits. In this manner, we avoid a fictitious reduction or enhancement of any baryon–meson loop by using an unappropriated value of the cutoff [28,38,39], as well as we prevent an arbitrary variation of the subtraction constants, as we correlate all of them with a UV cutoff [33].

The poles of the T matrix describe the odd-parity dynamically-generated Ξ_c and Ξ_b states, which appear in the first and second Riemann sheets (FRS and SRS). Poles of the scattering amplitude on the FRS below threshold are bound states, whereas poles on the SRS below the real axis and above threshold are resonances. The mass and the width of the bound state/resonance can be found from the position of the pole on the complex energy plane. At the complex pole, the T-matrix is given by

$$T_{ij}(s) = \frac{g_i g_j}{\sqrt{s} - \sqrt{s_R}} + \cdots, \quad (9)$$

where $\sqrt{s_R} = M_R - \mathrm{i}\,\Gamma_R/2$, with M_R the mass and Γ_R the width of the state, and g_i is the complex coupling of the state to the channel i, which is determined from Cauchy's theorem of residues. Thus, the dimensionless couplings g_i are obtained by first assigning an arbitrary sign to one of them (g_1), so

$$g_1^2 = \lim_{\sqrt{s} \to \sqrt{s_R}} (\sqrt{s} - \sqrt{s_R}) T_{11}(s). \quad (10)$$

The other couplings are calculated as,

$$g_j = g_1 \lim_{\sqrt{s} \to \sqrt{s_R}} \frac{T_{1j}(s)}{T_{11}(s)}, \quad (11)$$

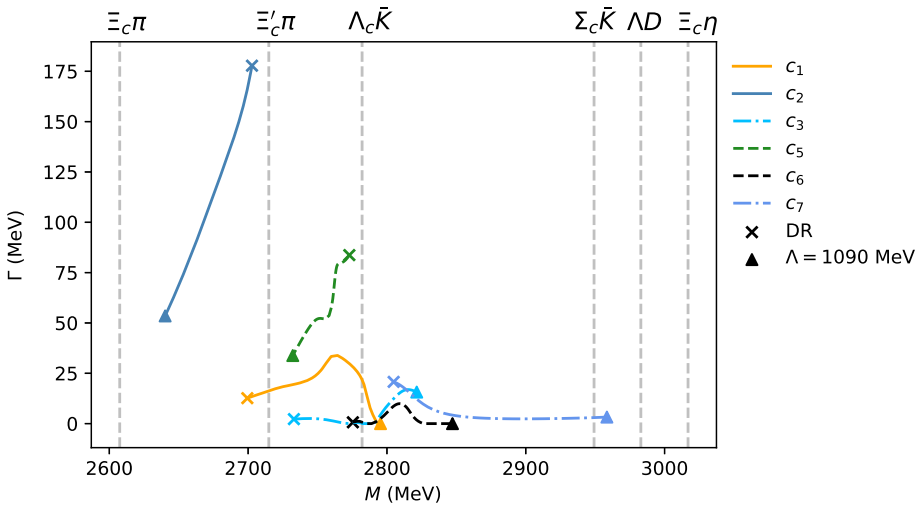

(a) $J = 1/2$

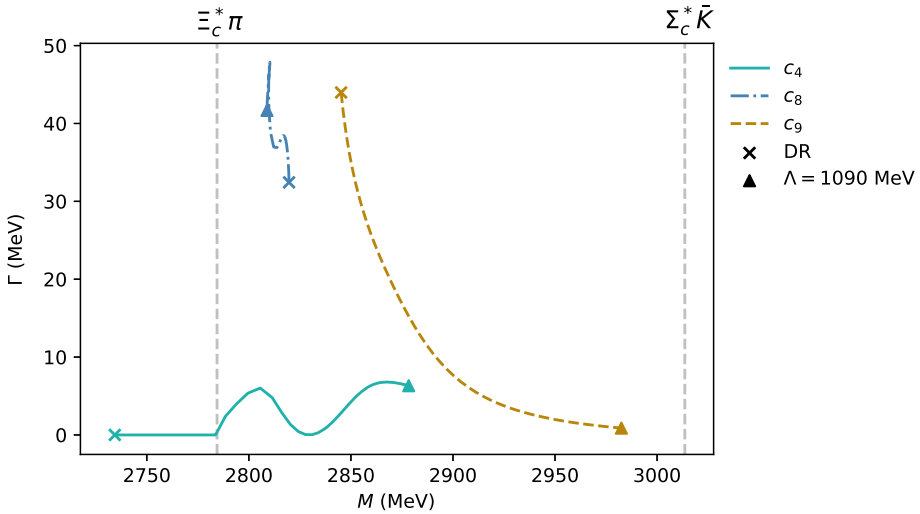

(b) $J = 3/2$

Fig. 1 Evolution of the masses and widths of the dynamically generated Ξ_c states as we vary the renormalization scheme from using a subtraction constant to a common cutoff of Λ =1090 MeV. The cross symbolizes the position of the states in the subtraction constant scheme [or dimensional regularization (DR)] [23], while the triangle indicates the mass and width of the same states for the cutoff scheme

and can be used to analyze the contribution of each baryon–meson channel to the generation of the state.

3 Results

3.1 Ξ_c excited states

As mentioned in the Introduction, the first observation of the $\Xi_c(2930)$ state was reported by the Belle Collaboration in Ref. [11]. This state was observed through its decay to $\Lambda_c^+ K^-$ with no assigned quantum numbers. Besides this recently discovered state, there are other three Ξ_c excited states with energies below 3 GeV [1]. As seen in Table 1, the $1/2^-$ $\Xi_c(2790)$ state decays into $\Xi_c'\pi$, whereas the $3/2^-$ $\Xi_c(2815)$ decays into $\Xi_c'\pi$ and has also the decay chain $\Xi_c^*\pi$, followed by $\Xi_c^* \to \Xi_c\pi$ [40]. Also, a $\Xi_c(2970)$ with unknown quantum numbers has been observed decaying into $\Lambda_c^+\bar{K}\pi$, $\Sigma_c\bar{K}$, $\Xi_c 2\pi$, $\Xi_c'\pi$ and $\Xi_c^*\pi$.

We start by revising the results Ref. [23] in the Ξ_c sector in order to understand whether the experimental states can be accommodated in our model. The widths of our Ξ_c states as a function of their masses in the $J = 1/2$ and $J = 3/2$ sectors are shown in the upper and lower plots of Fig. 1, respectively, together with different baryon–meson thresholds, to which they can couple. The dynamically generated states of Ref. [23] are displayed with a cross and the "DR" legend, as those have been obtained using one subtraction at certain scale or dimensional regularization. In what follows, we label the states as $c_1 \ldots c_9$, and they correspond to those given in Table V of Ref. [23]. They have either $J^P = 1/2^-$ or $J^P = 3/2^-$ and are ordered by their mass position. Hence, c_1 (c_9) corresponds to the lightest (heaviest) state of mass 2699.4 MeV (2845.2 MeV), among those quoted in the mentioned table, where their SU(6) and SU(3) quantum numbers are also given. We observe that the masses of our Ξ_c states using one subtraction constant (DR) are below or close to the

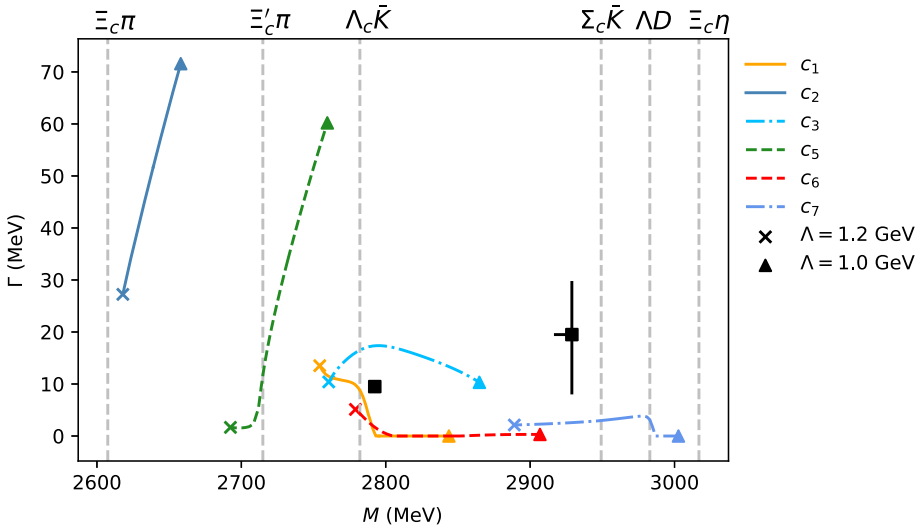

(a) $J = 1/2$

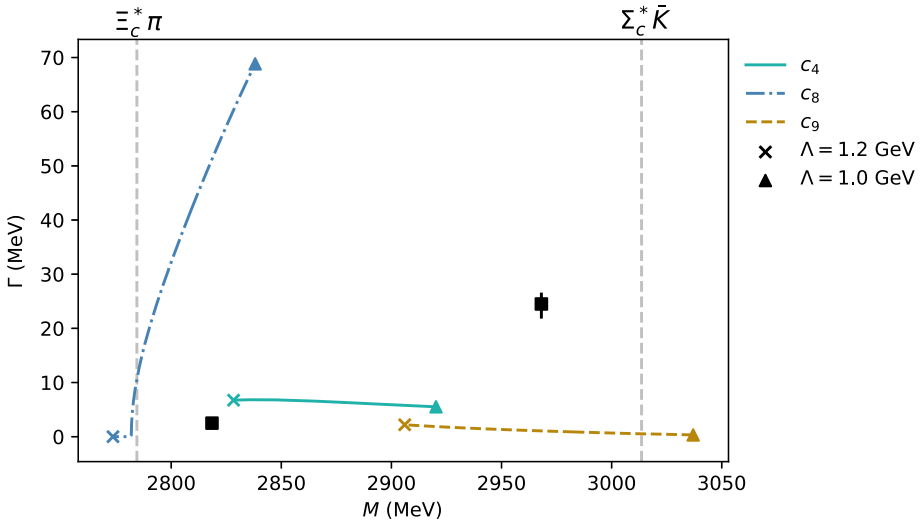

(b) $J = 3/2$

Fig. 2 Evolution of the masses and widths of the dynamically generated Ξ_c states, as we vary the cutoff from $\Lambda = 1$ GeV (triangles) to $\Lambda = 1.2$ GeV (crosses). In **a**, **b**, the c_1 (c_8) state becomes virtual above (below) the $\Lambda_c\overline{K}$ ($\Xi_c^*\pi$) threshold. The squares and their associated errorbars show the masses and widths of the experimental $\Xi_c(2790)$ and $\Xi_c(2930)$ (**a**) and $\Xi_c(2815)$ and $\Xi_c(2970)$ (**b**) together with their experimental errors. The spin–parity of both $\Xi_c(2930)$ and $\Xi_c(2970)$ resonances are not experimentally determined [1], and we have displayed them here just for illustrative purposes

experimental $\Xi_c(2790)$ or $\Xi_c(2815)$ states, while being far below in mass with respect to $\Xi_c(2930)$ or $\Xi_c(2970)$.

We then study the effect on masses and widths of the renormalization procedure so as to determine whether any our Ξ_c can be identified with a experimental state while assessing the dependence on the renormalization scheme, which might be significant (as shown in Ref. [28]). We proceed as described in Ref. [33] for the Ω_c states, where we explore a different renormalization procedure, the cutoff scheme. In order to do so, we first need to determine how the masses and widths of our dynamically generated states change as we adiabatically move from the one subtraction renormalization scheme to the cutoff one. Thus, we change the loop functions by

$$G_i^{\Lambda}(s) = \overline{G}_i(s) - (1-x)\,\overline{G}_i(\mu^2) + x\,\overline{G}_i^{\Lambda}(s), \qquad (12)$$

where we slowly evolve x from 0 to 1 while following the evolution of the states, as seen in Fig. 1. The c_1 to c_9 states for a $\Lambda = 1090$ MeV are shown with a triangle. We find that most of these states move to higher energies, except for c_2, c_5 and c_8, whereas getting closer to the experimental values. Note that fot this cutoff, the $J^P = 1/2^-$ c_1 state become virtual above the $\Lambda_c\bar{K}$ threshold.

Once we have identified our Ξ_c states in the cutoff scheme, we can assess the dependence of our results on this regulator, as well as their possible experimental identification. In Fig. 2 we show the evolution of the c_1 to c_9 states as we vary the cutoff from 1 GeV (triangles) to 1.2 GeV (crosses), and we also display different two-body thresholds. Moreover, in Table 2 we show masses and widths of the c_1 to c_9 states with $J = 1/2$ or $J = 3/2$, together with the couplings to the dominant baryon–meson channels ($g > 1$) and the couplings to

Table 2 Masses and widths of the c_1 to c_9 states with $J = 1/2$ or $J = 3/2$ and odd parity in the $C = 1$, $S = -1$ and $I = 1/2$ sector, together with the couplings (in modulus) to the dominant baryon–meson channels ($g > 1$) and the couplings to the decay channels reported experimentally for the Ξ_c states. All results have been obtained for $\Lambda = 1150$ MeV. We also indicate the possible experimental identification as well as the SU(6)$_{\rm lsf}\times$ HQSS, SU(6) and SU(3) irreducible representations of these states. We use the notation $\mathbf{R_{2J_C+1,C}}$, where $\mathbf{R}$ is the SU(6) irreducible representation (irrep) label (for which we use the dimension), J_C is the spin carried by the quarks with charm (1/2 in all cases) and C the charm content (1 in all cases). In addition, we also use $\mathbf{r_{2J+1}}$, where $\mathbf{r}$ is the SU(3) irrep, with J the total angular momentum of the state (see Ref. [23] for details)

Irreps	State	**M** (MeV)	**Γ** (MeV)	**J**	Couplings	Experiment
$(\mathbf{168}, \mathbf{21_{2,1}}, \mathbf{3_2^*})$	c_1	2773.59	10.52	1/2	$g_{\Xi_c\pi} = 0.5$, $g_{\Xi_c'\pi} = 0.3$, $g_{\Lambda_c\bar{K}} = 1.3$, $g_{\Sigma_c\bar{K}} = 0.9$, $g_{\Lambda D} = 1.6$, $g_{\Sigma D} = 1.5$, $g_{\Lambda D^*} = 2.9$, $g_{\Sigma D^*} = 1.0$, $g_{\Xi_c'\rho} = 1.0$, $g_{\Lambda_c\bar{K}^*} = 0.2$	$\Xi_c(2790)$
$(\mathbf{168}, \mathbf{15_{2,1}}, \mathbf{6_2})$	c_2	2627.5	38.84	1/2	$g_{\Xi_c\pi} = 1.8$, $g_{\Xi_c'\pi} = 0.04$, $g_{\Lambda_c\bar{K}} = 1.2$, $g_{\Sigma_c\bar{K}} = 0.1$, $g_{\Lambda_c\bar{K}^*} = 0.04$, $g_{\Sigma D} = 1.2$, $g_{\Lambda D^*} = 1.0$, $g_{\Sigma D^*} = 1.9$	
$(\mathbf{168}, \mathbf{21_{2,1}}, \mathbf{6_2})$	c_3	2790.99	16.09	1/2	$g_{\Xi_c\pi} = 0.3$, $g_{\Xi_c'\pi} = 0.8$, $g_{\Lambda_c\bar{K}} = 0.2$, $g_{\Sigma_c\bar{K}} = 1.7$, $g_{\Sigma D} = 2.6$, $g_{\Lambda D^*} = 2.2$, $g_{\Xi_c'\eta} = 1.1$, $g_{\Lambda_c\bar{K}^*} = 1.0$, $g_{\Sigma D^*} = 2.3$, $g_{\Sigma_c\bar{K}^*} = 1.1$, $g_{\Xi D_s^*} = 1.7$	
$(\mathbf{168}, \mathbf{21_{2,1}}, \mathbf{6_4})$	c_4	2850.89	6.76	3/2	$g_{\Xi_c^*\pi} = 0.6$, $g_{\Sigma_c^*\bar{K}} = 2.2$, $g_{\Lambda_c\bar{K}^*} = 1.5$, $g_{\Xi_c^*\eta} = 1.1$, $g_{\Sigma^* D} = 1.1$, $g_{\Sigma^* D^*} = 1.5$, $g_{\Sigma_c^*\bar{K}^*} = 1.8$	$\Xi_c(2815)$
$(\mathbf{168}, \mathbf{15_{2,1}}, \mathbf{3_2^*})$	c_5	2715.23	12.28	1/2	$g_{\Xi_c\pi} = 0.2$, $g_{\Xi_c'\pi} = 1.8$, $g_{\Lambda_c\bar{K}} = 0.5$, $g_{\Sigma_c\bar{K}} = 1.2$, $g_{\Lambda D} = 3.1$, $g_{\Lambda_c\bar{K}^*} = 0.1$, $g_{\Sigma D} = 1.5$	
$(\mathbf{120}, \mathbf{21_{2,1}}, \mathbf{3_2^*})$	c_6	2807	1.82	1/2	$g_{\Xi_c\pi} = 0.1$, $g_{\Xi_c'\pi} = 0.1$, $g_{\Lambda_c\bar{K}} = 0.2$ $g_{\Sigma_c\bar{K}} = 1.4$, $g_{\Sigma D} = 1.6$, $g_{\Lambda D^*} = 1.1$, $g_{\Sigma D^*} = 4.3$, $g_{\Xi D_s} = 1.1$, $g_{\Sigma_c\bar{K}^*} = 1.4$, $g_{\Xi D_s^*} = 1.9$	
$(\mathbf{120}, \mathbf{21_{2,1}}, \mathbf{6_2})$	c_7	2922.5	2.48	1/2	$g_{\Xi_c\pi} = 0.2$, $g_{\Xi_c'\pi} = 0.03$, $g_{\Lambda_c\bar{K}} = 0.2$, $g_{\Sigma_c\bar{K}} = 0.1$, $g_{\Lambda D} = 1.8$, $g_{\Sigma D} = 1.4$, $g_{\Lambda D^*} = 1.7$, $g_{\Lambda_c\bar{K}^*} = 1.2$, $g_{\Sigma D^*} = 1.5$, $g_{\Xi_c\rho} = 1.2$, $g_{\Sigma^* D^*} = 3.7$, $g_{\Sigma_c\bar{K}^*} = 1.1$, $g_{\Xi_c^*\rho} = 1.0$, $g_{\Xi^* D_s^*} = 1.9$	$\Xi_c(2930)$
$(\mathbf{168}, \mathbf{15_{2,1}}, \mathbf{3_4^*})$	c_8	2792.06	22.79	3/2	$g_{\Xi_c^*\pi} = 1.7$, $g_{\Sigma_c^*\bar{K}} = 1.0$, $g_{\Lambda D^*} = 2.4$, $g_{\Sigma D^*} = 1.2$, $g_{\Lambda_c\bar{K}^*} = 0.2$	
$(\mathbf{120}, \mathbf{21_{2,1}}, \mathbf{6_4})$	c_9	2942.05	1.46	3/2	$g_{\Xi_c^*\pi} = 0.2$, $g_{\Sigma_c^*\bar{K}} = 0.2$, $g_{\Lambda_c\bar{K}^*} = 0.4$, $g_{\Lambda D^*} = 2.7$, $g_{\Sigma D^*} = 2.2$, $g_{\Sigma^* D} = 2.8$, $g_{\Sigma^* D^*} = 3.4$, $g_{\Xi^* D_s} = 1.4$, $g_{\Xi^* D_s^*} = 1.8$	$\Xi_c(2970)$

the decay channels reported experimentally for the Ξ_c states. All these results are obtained for $\Lambda = 1150$ MeV. In this table we also indicate the possible experimental identification as well as the SU(6)$_{\rm lsf}\times$HQSS, SU(6) and SU(3) irreducible representations (irreps), to which the c_1 to c_9 states belong (see Ref. [23] for group-structure details).

As we evolve the cutoff value from $\Lambda = 1000$ MeV to $\Lambda = 1200$ MeV, that is, from the right to left in Fig. 2, we observe that some of our dynamically generated resonances can be identified with the experimental states attending to the complex energy position.

In the $J^P = 1/2^-$ sector, attending to the position in the complex plane, we observe that the $\Xi_c(2790)$ could be one of the c_1, c_3, c_6 or even the c_5 states. The identification with the $\Xi_c(2790)$ is possible because these states couple to $\Xi_c'\pi$, although this baryon–meson channel is not the dominant one for their dynamically generation, as seen in Table 2 for a $\Lambda = 1150$ MeV, except for c_5. Indeed, this latter feature of c_5 disfavors its identification with the $\Xi_c(2790)$. This is because it would become too broad ($\Gamma \geq 70$ MeV) for UV cutoffs of around 1 GeV, that would lead the c_5 resonance to have masses closer to the experimental one, as seen in Fig. 2. In addition in the DR scheme, the mass of the c_5 state is close to 2790 MeV, but its width is approximately of 84 MeV [23] (see also Fig. 1), while experimentally $\Gamma_{\Xi_c(2790)} \sim 10$ MeV.

Looking at the behavior of the c_1, c_3, c_6 poles with the UV cutoff in Fig. 2, it seems natural to assign the $\Xi_c(2790)$ to the c_1 pole. This state has a width of the order of 10 MeV for UV cutoffs in the region of 1.2 GeV, where it is located below the $\Lambda_c\bar{K}$ threshold. At the same time, the state has large $\Lambda_c\bar{K}$ and small $\Xi_c'\pi$ couplings (see Table 2), respectively, which explains its small experimental width despite being placed well above the latter threshold, and it is natural to think that the $\Lambda_c\bar{K}$ channel should play an important role in the dynamics of the $\Xi_c(2790)$ given its proximity to that threshold. Note that the light degrees of freedom (*ldof*) in the inner structure of the c_1 are predominantly coupled to $j^\pi_{ldof} = 0^-$ spin–parity quantum numbers [28]. Thus with

this identification, this first odd parity excited Ξ_c state would not have a dominant configuration consisting of a spinless light diquark and a unit of angular momentum between it and the heavy quark, as argued for instance in the Belle Collaboration paper [40]. This is to say, the $\Xi_c(2790)$ will not be a constituent quark model λ-mode excited state [28,41] with $j^{\pi}_{ldof} = 1^-$ and hence it will not form part of any HQSS doublet, thus making the assignment to c_3 unlikely. Actually, if the spin–parity quantum numbers for the *ldof* in the $\Xi_c(2790)$ were predominantly 1^-, one would expect a larger width for this resonance, since its decay to the open channel $\Xi_c'\pi$ is HQSS allowed. This is precisely the situation for the c_3 that is broader than the experimental state. In summary, we conclude a large molecular $\Lambda_c\bar{K}$ component for the $\Xi_c(2790)$ that will have then a dominant $j^{\pi}_{ldof} = 0^-$ configuration.

Our present $\Xi_c(2790)$ identification with the c_1 pole differs from the previous assignments in Ref. [23], where the Ξ_c states were obtained using the one subtraction renormalization scheme. In this previous work, the c_7 state was assigned to $\Xi_c(2790)$ due to its closeness in energy and the sizable $\Xi_c'\pi$ coupling within the DR scheme.

With regards to the recently discovered $\Xi_c(2930)$, if we assume that this state has $J^P = 1/2^-$, we could identify it either with our c_6 or c_7 states, as they both couple to the $\Lambda_c\bar{K}$ channel, although not dominantly as seen in Table 2 for a $\Lambda = 1150$ MeV. The assignment to the c_6 pole is, however, disfavored because of the mass difference between this state and the experimental $\Xi_c(2930)$. As for c_7, the small $\Lambda_c\bar{K}$ coupling of this state makes also somehow doubtful its identification with the $\Xi_c(2930)$. In the case of our c_2 and c_5 states, we should mention that we do not have any clear experimental candidate at this point for the c_5 dynamically generated $J = 1/2$ state, whereas the c_2 state becomes broad and appears below 2650 MeV, thus not allowing for any reasonable experimental assignment.

For $J^P = 3/2^-$, the analysis of the evolution of the different states in Fig. 2 allows for the identification of the experimental $\Xi_c(2815)$ with c_4 or c_8. These states couple to $\Xi_c^*\pi$ in S-wave, although for c_4, couplings to other baryon–meson states ($\Sigma_c^*\bar{K}$, $\Lambda_c\bar{K}^*$ or $\Sigma_c^*\bar{K}^*$) are larger as seen in Table 2. The experimental $\Xi_c(2815)$ is quite narrow, $\Gamma_{\Xi_c(2815)} \sim 2-3$ MeV, despite the $\Xi_c^*\pi$ threshold being around 30 MeV below its mass. This hints to a subdominant $\Xi_c^*\pi$ molecular component in the inner structure of this resonance. Moreover, looking at the dependence of the $J^P = 3/2^-$ pole masses and widths with the UV cutoff displayed in Fig. 2, it seems reasonable to assign the c_4 state to the $\Xi_c(2815)$ resonance.

As for $\Xi_c(2970)$, assuming that it has $J = 3/2^-$, we could identify it with the c_9 state for values of the cutoff around $\Lambda \simeq 1.1$ GeV. In this case, we have to take into account that this state couples to $\Lambda_c\bar{K}^*$ and $\Sigma_c^*\bar{K}$, and $\Xi_c^*\pi$ (though not dominantly), and those baryon–meson channels can decay into $\Lambda_c\bar{K}\pi$ and $\Xi_c\pi\pi$, respectively. Nevertheless, the predicted width would be significantly smaller than the range of 20-30 MeV quoted in the PDG [1] and shown in Table 1. Compared to the results of Ref. [23], the $\Xi_c(2815)$ was identified there with c_9, assuming that $\Xi_c(2790)$ and $\Xi_c(2815)$ were the c_7 and c_9 HQSS partners.

In fact, we observe several HQSS partners among our states as well as possible siblings within the same $SU(3)$ representation. The $\Xi_c(2790)$ resonance belongs to an $J = 1/2$ SU(3) antitriplet irrep, and it would be the SU(6)$_{\rm lsf}\times$HQSS (see Table 2) partner of a narrow Λ_c^* state discussed in [21,23,28]. This latter state has large (small) ND and ND^* ($\Sigma_c\pi$) couplings, and depending on the renormalization scheme (one-subtraction or UV cutoff), it is part of a double pole pattern for the $\Lambda_c(2595)$, similar to that found for the $\Lambda(1405)$ within unitarized chiral models [29,30,42–47] (see related review in [1]), or it is located in the region of 2.8 GeV close to the ND threshold [28].

On the other hand, the c_3 pole belonging to (**168**, **21**, $\mathbf{6_2}$) representation and the c_4 of the (**168**, **21**, $\mathbf{6_4}$) form a ($j^{\pi}_{ldof} = 1^-$)-HQSS doublet. As mentioned earlier, the c_4 can be identified with the $\Xi_c(2815)$, but we note that the $\Xi_c(2815)$ is not the sibling of the $\Lambda_c(2625)$ because of the different coupling strengths to $\Xi_c^*\pi$ and $\Sigma_c^*\pi$, respectively. Whereas $\Xi_c(2815)$ weakly couples to $\Xi_c^*\pi$, the $\Lambda_c(2625)$ strongly does to $\Sigma_c^*\pi$. However, this latter state is narrow because the $\Sigma_c^*\pi$ channel is closed (located around 30 MeV above the mass of the resonance). Indeed, recently it has been argued that the $\Lambda(2625)$ is probably a constituent three quark state [28,41].

As for the $J = 1/2$ c_5 and the $J = 3/2$ c_8 states, those form part of a SU(6) **15**-plet, belonging to the SU(6)$_{\rm lsf}\times$ HQSS (**168**, **15**, $\mathbf{3_2}$) and (**168**, **15**, $\mathbf{3_4}$) irreps [23]. They form a HQSS doublet with $j^{\pi}_{dof} = 1^-$ and hence have large couplings to $\Xi_c'\pi$ and $\Xi_c^*\pi$, respectively. Indeed, as a good approximation, they are dynamically generated by the charmed baryon–Goldstone boson interactions. These moderately broad states are in the SU(3)$_{2J+1}$ $\mathbf{3_2^*}$ and $\mathbf{3_4^*}$ irreps, which should be completed by one $J = 1/2$ and one $J = 3/2$ Λ_c resonances stemming from the $\Sigma_c\pi$ and $\Sigma_c^*\pi$ chiral interactions [19,28], neglecting higher energy channels. The $J = 3/2$ sibling is, however, not the $\Lambda_c(2625)$. As mentioned before, the $\Lambda_c(2625)$ is probably a quark model (λ-mode excitation) state [28,41]. Another resonance with mass and width of around 2.7 GeV and 60 MeV [19,28], that has not been discovered yet, would then be the SU(3) sibling of the c_8 state.

The features of the $J = 1/2$ counterpart of c_5 in the Λ_c sector are much more uncertain and depend on both the employed renormalization scheme and on the interplay between quark-model and baryon–meson degrees of freedom [28]. Thus, for instance neglecting the latter, it would appear

Table 3 Masses and widths of the b_1 to b_9 states with $J = 1/2$ or $J = 3/2$ in the $B = -1$, $S = -1$ and $I = 1/2$ sector, together with the couplings to the dominant baryon–meson channels and the couplings to the experimental decay channels of the $\Xi_b(6227)$, using one-subtraction renormalization, as in Table IV of Ref. [24]. We also indicate the $SU(6)_{lsf} \times$ HQSS, SU(6) and SU(3) irreducible representations of these states, as in Table 2. States with $*$ are virtual states. Note that the b_8^* lies in the real axis, but in a sheet that is not connected to the physical sheet, thus we are not showing the couplings indicating "R.S (real sheet) not connected"

Irreps	State	$\mathbf{M_R}$ (MeV)	Γ_R (MeV)	J	Couplings
$(\mathbf{168}, \mathbf{21}_{2,1}, \mathbf{3}_2^*)$	b_1	5873.98	0	1/2	$g_{\Lambda\bar{B}} = 1.3$, $g_{\Sigma\bar{B}} = 4.4$, $g_{\Lambda\bar{B}^*} = 2.3$, $g_{\Sigma\bar{B}^*} = 7.3$, $g_{\Xi\bar{B}_s} = 2.6$, $g_{\Xi_b\eta'} = 1.0$, $g_{\Xi\bar{B}_s^*} = 4.5$
$(\mathbf{168}, \mathbf{15}_{2,1}, \mathbf{6}_2)$	b_2	5940.85	35.59	1/2	$g_{\Xi_b\pi} = 1.8$, $g_{\Lambda\bar{B}} = 3.7$, $g_{\Lambda\bar{B}^*} = 6.2$, $g_{\Sigma\bar{B}^*} = 1.6$, $g_{\Xi\bar{B}_s} = 1.1$, $g_{\Xi\bar{B}_s^*} = 1.9$
$(\mathbf{168}, \mathbf{21}_{2,1}, \mathbf{6}_2)$	b_3	5880.76	0	1/2	$g_{\Lambda\bar{B}} = 2.5$, $g_{\Sigma\bar{B}} = 2.4$, $g_{\Lambda\bar{B}^*} = 1.3$, $g_{\Sigma\bar{B}^*} = 1.6$, $g_{\Xi\bar{B}_s} = 1.7$, $g_{\Sigma^*\bar{B}^*} = 8.0$, $g_{\Xi_b'\eta'} = 1.0$, $g_{\Xi^*\bar{B}_s^*} = 4.9$
$(\mathbf{168}, \mathbf{21}_{2,1}, \mathbf{6}_4)$	b_4	5880.27	0	3/2	$g_{\Lambda\bar{B}^*} = 2.8$, $g_{\Sigma\bar{B}^*} = 2.8$, $g_{\Sigma^*\bar{B}} = 5.0$, $g_{\Sigma^*\bar{B}^*} = 6.3$, $g_{\Xi\bar{B}_s^*} = 1.8$, $g_{\Xi^*\bar{B}_s} = 3.1$, $g_{\Xi_b^*\eta'} = 1.0$, $g_{\Xi^*\bar{B}_s^*} = 3.9$
$(\mathbf{168}, \mathbf{15}_{2,1}, \mathbf{3}_2^*)$	b_5^*	5949.93	0.7	1/2	$g_{\Xi_b'\pi} = 1.4$, $g_{\Lambda\bar{B}} = 6.2$, $g_{\Lambda\bar{B}^*} = 3.8$, $g_{\Sigma^*\bar{B}^*} = 1.6$, $g_{\Xi^*\bar{B}_s^*} = 2.2$
$(\mathbf{120}, \mathbf{21}_{2,1}, \mathbf{3}_2^*)$	b_6	6034.80	28.8	1/2	$g_{\Xi_b\pi} = 1.0$, $g_{\Lambda_b\bar{K}} = 2.0$, $g_{\Lambda\bar{B}} = 1.0$, $g_{\Lambda\bar{B}^*} = 2.1$, $g_{\Sigma\bar{B}^*} = 1.1$, $g_{\Xi\bar{B}_s} = 1.3$, $g_{\Xi\bar{B}_s^*} = 2.1$
$(\mathbf{120}, \mathbf{21}_{2,1}, \mathbf{6}_2)$	b_7	6035.39	0.02	1/2	$g_{\Sigma_b\bar{K}} = 2.3$, $g_{\Lambda\bar{B}} = 1.0$, $g_{\Sigma\bar{B}} = 4.5$, $g_{\Sigma\bar{B}^*} = 2.8$, $g_{\Xi_b\omega} = 1.2$, $g_{\Sigma^*\bar{B}^*} = 2.3$
$(\mathbf{168}, \mathbf{15}_{2,1}, \mathbf{3}_4^*)$	b_8^*	5958.20	0	3/2	– R.S. not connected –
$(\mathbf{120}, \mathbf{21}_{2,1}, \mathbf{6}_4)$	b_9	6043.28	0	3/2	$g_{\Sigma_b^*\bar{K}} = 2.3$, $g_{\Lambda\bar{B}^*} = 1.1$, $g_{\Sigma\bar{B}^*} = 5.5$, $g_{\Sigma^*\bar{B}} = 1.5$, $g_{\Xi_b\omega} = 1.2$, $g_{\Sigma^*\bar{B}^*} = 1.7$

around 2.6 GeV with a large width of 60-80 MeV because its sizable coupling to the $\Sigma_c\pi$ pair. Within the UV cutoff RS, this state can be easily moved below the $\Sigma_c\pi$ threshold and be identified with the narrow $\Lambda_c(2595)$ [19]. In the DR scheme advocated in Ref. [23], this broad state, together with the $j^\pi_{ldof} = 0^-$ narrow state mentioned above in the discussion of the $\Xi_c(2790)$, gives rise to a double pole structure for the $\Lambda_c(2595)$.

Within the UV cutoff renormalization scheme examined here, the (c_7, c_9) HQSS-doublet might correspond to the experimental $\Xi_c(2930)$ and $\Xi_c(2970)$ states. The c_7 state, that we have tentatively assigned to the $\Xi_c(2930)$, exhibits (Table 2) moderate couplings to $\Xi_c\pi$ and $\Lambda_c\bar{K}$, small ones to $\Xi_c'\pi$ and $\Sigma_c\bar{K}$, and finally large couplings to $\Lambda D^{(*)}$, $\Sigma D^{(*)}$ and $\Sigma^* D^*$. It belongs to a SU(3) sextet, where there is also a Ω_c state. The latter corresponds to the one labeled as **d** in our previous study of the Ω_c odd-parity resonances [33], where it was tentatively assigned either to the $\Omega_c(3090)$ or the $\Omega_c(3119)$ observed by the LHCb Collaboration in the $\Xi_c\bar{K}$ mode [8]. This is in fact consistent with what one might expect from its c_7-sibling couplings. Assuming the *equal spacing rule* we could predict the possible existence of a $J = 1/2^-$ Σ_c state around 2800 MeV that will complete the sextet. The $\Sigma_c(2800)$ clearly fits into this picture since it is observed in the $\Lambda_c\pi$ channel [1].

Recently there has been an analysis of the Ξ_c sector within a baryon–meson molecular model based on local hidden gauge that implements the interaction between the $1/2^+$ and $3/2^+$ ground-state baryons with 0^- and 1^- mesons [18]. The authors have found that five of their dynamically generated Ξ_c states can be identified with the experimental $\Xi_c(2790)$, $\Xi_c(2930)$, $\Xi_c(2970)$, $\Xi_c(3055)$ and $\Xi_c(3080)$. Whereas the $\Xi_c(2790)$ would be a $1/2^-$ state, the $\Xi_c(2930)$, $\Xi_c(2970)$, $\Xi_c(3055)$ and $\Xi_c(3080)$ could be either $1/2^-$ or $3/2^-$ ones. Compared to this approach, our model identifies the experimental $\Xi_c(2790)$ and $\Xi_c(2930)$ as $1/2^-$ states, and the $\Xi_c(2815)$ and $\Xi_c(2970)$ as $3/2^-$. The different assignment is mainly due the distinct renormalization scheme used in the two approaches as well as the fact the interactions involving D and D^* and light vector mesons with baryons are not completely fixed by HQSS or chiral symmetries, thus allowing for different assumptions.

3.2 Ξ_b excited states

With regards to the bottom sector, the $\Xi_b(6227)$ resonance has been recently measured by the LHCb experiment [9], with $\Gamma_{\Xi_b(6227)} \sim 18$ MeV. Its quantum numbers, though, remain unknown, whereas the observed decay channels are $\Lambda_b^0 K^-$ and $\Xi_b^0\pi^-$ (see Table 1).

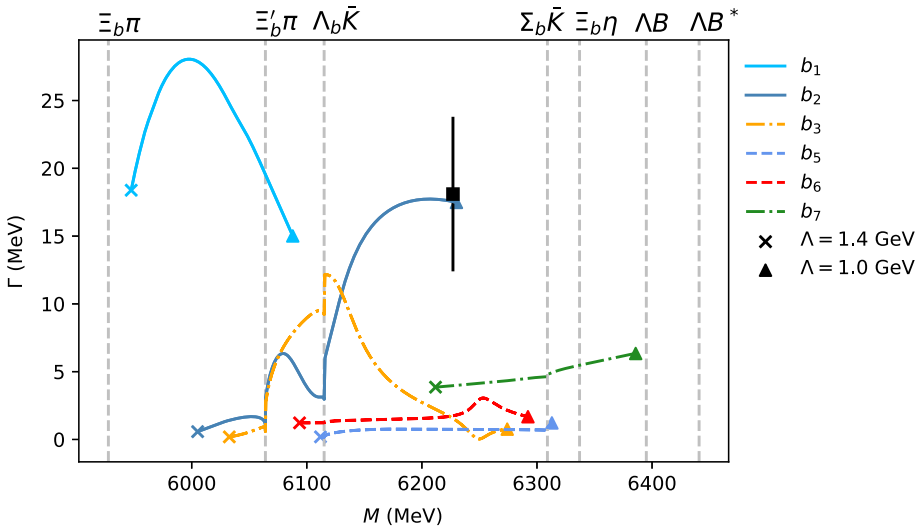

(a) $J = 1/2$

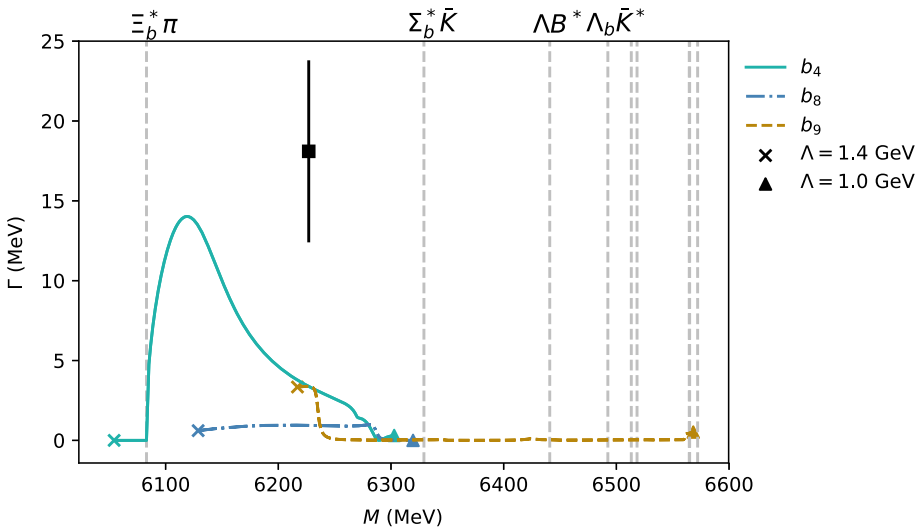

(b) $J = 3/2$

Fig. 3 Evolution of the masses and widths of the dynamically generated Ξ_b states, as we vary the cutoff from $\Lambda = 1000$ MeV (triangles) to $\Lambda = 1400$ MeV (crosses), with $J = 1/2$ (upper panel) and $J = 3/2$ (lower panel). The square and its bars represent the position of the $\Xi_b(6227)$ resonance, and its errors in mass and width, respectively. We show the experimental result for both values of J due to its unknown quantum numbers. In **b**, the last five thresholds (not labelled in the figure because they are too close to each other) are: $\Xi_b^*\eta$ (6492.45 MeV), ΣB^* (6518.35 MeV), $\Omega_b K$ (6564.68 MeV), $\Xi_b\rho$ (6565.04 MeV) and $\Xi_b\omega$ (6572.12 MeV)

We start again by revising the previous results of Ref. [24] with $B = -1$, $S = -1$, $I = 1/2$ (Ξ_b sector). Masses and widths of the dynamically generated states within our model using the DR scheme, together with their irreps, spins and couplings to the dominant baryon–meson channels as well those for the experimental decay channels of $\Xi_b(6227)$ are shown in Table 3. We obtain nine states, which are the bottom counterparts of the Ξ_c ones discussed in the previous subsection. Compared to Ref. [24], we report here five more poles, since in that reference only SU(3) flavor partners of Λ_b states were searched (members of antitriplet irreps). Also, two of them, the state at 6035 MeV with $J = 1/2$ and the one at 6043 MeV with $J = 3/2$ were wrongly assigned in Ref. [24] to the SU(6) **15** representation. Instead, their should belong to the SU(6) **21** representation, as seen in Table 3. Moreover, there is a state at 6073 MeV in Table IV in Ref. [24] that does not appear in our present calculation. The differences between of them are due to the difficulty in determining the number of states and their representations as we break the $SU(6)_{lsf} \times$HQSS symmetry to SU(3) in the bottom sector, as almost all states have zero width and states with widths closer to zero are more difficult to follow in the complex energy plane.

As in the Ξ_c sector, our b_1 to b_9 states using one-subtraction renormalization are too low in energy so as to assign any of them to the experimental $\Xi_b(6227)$ state. Thus, we proceed as in the previous subsection and vary the renormalization scheme from one-subtraction to cutoff. In this manner, we identify our b_1 to b_9 states using one-subtraction renormalization with the ones within the cutoff scheme, and we study their evolution as we change the value of the cutoff.

In Fig. 3 we display the evolution of the masses and widths of the dynamically generated Ξ_b states as we vary the cutoff from $\Lambda = 1000$ MeV (triangles) to $\Lambda = 1400$ MeV, for

Table 4 As Table 2, but for the Ξ_b sector ($\Lambda = 1150$ MeV)

Irreps	State	M_R (MeV)	Γ_R (MeV)	J	Couplings	Experiment
$(\mathbf{168}, \mathbf{21}_{2,1}, \mathbf{3}^*_2)$	b_1	6025.46	25.88	1/2	$g_{\Xi_b\pi} = 0.94$, $g_{\Lambda_b\bar{K}} = 1.4$, $g_{\Xi_b\eta} = 2.1$, $g_{\Sigma\bar{B}} = 1.4$, $g_{\Sigma\bar{B}^*} = 2.6$, $g_{\Xi\bar{B}^*_s} = 1.3$	
$(\mathbf{168}, \mathbf{15}_{2,1}, \mathbf{6}_2)$	b_2	6152.61	15.29	1/2	$g_{\Xi_b\pi} = 0.33$, $g_{\Lambda_b\bar{K}} = 0.51$, $g_{\Sigma_b\bar{K}} = 0.40$, $g_{\Lambda\bar{B}} = 1.9$, $g_{\Sigma\bar{B}} = 2.1$, $g_{\Lambda\bar{B}^*} = 7.3$, $g_{\Xi\bar{B}_s} = 1.6$	$\Xi_b(6227)$
$(\mathbf{168}, \mathbf{21}_{2,1}, \mathbf{6}_2)$	b_3	6179.4	3.81	1/2	$g_{\Xi_b\pi} = 0.05$, $g_{\Lambda_b\bar{K}} = 0.1$, $g_{\Lambda\bar{B}} = 1.08$, $g_{\Sigma\bar{B}} = 1.92$, $g_{\Lambda\bar{B}^*} = 1.87$, $g_{\Omega_b K} = 2.26$, $g_{\Xi\bar{B}_s} = 5.13$, $g_{\Xi\bar{B}^*_s} = 2.65$, $g_{\Xi_b\phi} = 2.29$, $g_{\Omega_b K^*} = 1.04$, $g_{\Xi'_b\phi} = 1.15$	
$(\mathbf{168}, \mathbf{21}_{2,1}, \mathbf{6}_4)$	b_4	6202.73	4.48	3/2	$g_{\Lambda\bar{B}^*} = 2.3$, $g_{\Sigma\bar{B}^*} = 1.5$, $g_{\Omega_b K} = 2.2$, $g_{\Xi\bar{B}^*_s} = 5.5$, $g_{\Xi_b\phi} = 2.3$, $g_{\Omega_b\bar{K}^*} = 1.2$, $g_{\Xi^*_b\phi} = 1.3$	
$(\mathbf{168}, \mathbf{15}_{2,1}, \mathbf{3}^*_2)$	b_5	6243.02	0.74	1/2	$g_{\Xi_b\pi} = 0.02$, $g_{\Lambda_b\bar{K}} = 0.12$, $g_{\Sigma_b\bar{K}} = 0.48$, $g_{\Sigma\bar{B}} = 1.8$, $g_{\Sigma\bar{B}^*} = 6.9$	
$(\mathbf{120}, \mathbf{21}_{2,1}, \mathbf{3}^*_2)$	b_6	6212.26	1.6	1/2	$g_{\Xi_b\pi} = 0.05$, $g_{\Lambda_b\bar{K}} = 0.01$, $g_{\Sigma_b\bar{K}} = 1.2$, $g_{\Lambda\bar{B}} = 1.3$, $g_{\Sigma\bar{B}} = 4.9$, $g_{\Lambda\bar{B}^*} = 2.3$, $g_{\Xi'_b\eta} = 1.6$	
$(\mathbf{120}, \mathbf{21}_{2,1}, \mathbf{6}_2)$	b_7	6327.28	5.29	1/2	$g_{\Xi_b\pi} = 0.01$, $g_{\Lambda_b\bar{K}} = 0.02$, $g_{\Lambda\bar{B}} = 1.4$, $g_{\Sigma\bar{B}} = 1.3$, $g_{\Lambda\bar{B}^*} = 1.2$, $g_{\Lambda_b\bar{K}^*} = 1.9$, $g_{\Sigma\bar{B}^*} = 1.3$, $g_{\Xi_b\rho} = 1.5$, $g_{\Sigma^*\bar{B}^*} = 2.2$	
$(\mathbf{168}, \mathbf{15}_{2,1}, \mathbf{3}^*_4)$	b_8	6240.82	0.92	3/2	$g_{\Xi^*_b\pi} = 0.15$, $g_{\Sigma^*_b\bar{K}} = 1.3$, $g_{\Lambda\bar{B}^*} = 2.0$, $g_{\Xi^*_b\eta} = 1.5$, $g_{\Sigma\bar{B}^*} = 4.8$	
$(\mathbf{120}, \mathbf{21}_{2,1}, \mathbf{6}_4)$	b_9	6459.42	0.02	3/2	$g_{\Xi^*\bar{B}_s} = 4.5$, $g_{\Omega_b K^*} = 2.2$, $g_{\Xi'_b\phi} = 3.0$, $g_{\Xi^*\bar{B}^*_s} = 3.0$, $g_{\Omega_b\bar{K}^*} = 1.0$, $g_{\Xi^*_b\phi} = 1.3$	

$J = 1/2$ (upper plot) and $J = 3/2$ (lower plot). The square and its bar represent the position of the $\Xi_b(6227)$ resonance, and the error for its mass and width, respectively. We show the experimental result ($\Xi_b(6227)$) for both $J = 1/2$ and $J = 3/2$ because its quantum numbers have not been determined yet. Additionally, in Table 4, we collect the masses and the widths of the b_1 to b_9 states with $J = 1/2$ or $J = 3/2$, together with the couplings to the dominant baryon–meson channels and the couplings to the decay channels of the $\Xi_b(6227)$, for $\Lambda = 1150$ MeV as in the charm sector. We also indicate the SU(6)$_{\rm lsf}\times$ HQSS, SU(6) and SU(3) irreducible representations of these states.

We might try now to assign the experimental $\Xi_b(6227)$ to any of our states, while determining the negative parity baryons with $B = -1$ belonging to the same $\mathbf{3}^*$ and $\mathbf{6}$ SU(3) representations. The observed decay modes, $\Lambda^0_b K^-$, $\Xi^0_b\pi^-$ [9], of the resonance support that this state should have $1/2^-$ spin–parity, assuming S-wave. Moreover, the $j^\pi_{ldof} = 0^-$ component should be also quite relevant, which according to the couplings collected in Table 4 makes plausible its identification either with the b_1 or b_2 states. The evolution displayed in the upper plot of Fig. 3 leads us to assign the $\Xi_b(6227)$ to the b_2 state, as shown in Table 4. The b_2 pole would stem from a SU(6) **15**-plet, composed of $J = 1/2$ and $J = 3/2$ SU(3) antitriplets and of a $J = 1/2$ SU(3) sextet, where the $\Xi_b(6227)$ would be accommodated. The $J = 1/2^-$ $\Lambda_b(5912)$ and $J = 3/2^-$ $\Lambda_b(5920)$ (LHCb [32]) would be part of the $\mathbf{3}^*_\mathbf{2}$ and $\mathbf{3}^*_\mathbf{4}$ multiplets forming a HQSS-doublet [24]. These antitriplets should be completed by another HQSS-doublet of Ξ_b and Ξ^*_b states, b_5 and b_8, that according to Fig. 3 and Table 4 should have masses around 6250 MeV and could be seen in the $\Sigma_b^{(*)}\bar{K}$ and $\Xi_b^{(\prime *)}\pi$ modes.

Coming back to the $\Xi_b(6227)$, it belongs to a $j^\pi_{ldof} = 0^-$−sextet that should be completed by $J = 1/2$ Σ_b and Ω_b states. The recent $\Sigma_b(6097)$ resonance seen by the LHCb Collaboration [48] in the $\Lambda_b\pi$ channel nicely fits in this multiplet. Relying again in the *equal spacing rule*, we could foresee the existence of a $J = 1/2$ Ω_b odd parity state with a mass of around 6360 MeV that should be observed in the $\Xi_b\bar{K}$ channel. Some molecular Ω_b states were predicted previously in Ref. [49], but all of them above 6.4 GeV.

Previous works based on molecular approaches have also found the $\Xi_b(6227)$ as a dynamically-generated state. In Refs. [19,20] a unitarized model using the leading-order chiral Lagrangian found the $\Xi_b(6227)$ as a S-wave $\Sigma_b\bar{K}$ molecule, with a preferred $1/2^-$ spin–parity assignment [20]. In our present model the $\Lambda\bar{B}^*$, $\Sigma\bar{B}$ and $\Lambda\bar{B}$ are the dominant channels in the generation of the $\Xi_b(6227)$, though it also couples (weakly) to $\Sigma_b\bar{K}$. The main difference between models comes from the fact that our scheme has a more extensive number of channels, whereas the antitriplet and sextet multiplets of ground-state baryons mix when constructing the interaction matrices. Also, the work of Ref. [18] has also analyzed the Ξ_b sector. The authors have found two poles with masses close to the $\Xi_b(6227)$ and widths $\sim 25 - 30$ MeV, close to the experimental one, with $1/2^-$ and $3/2^-$

Fig. 4 Bottom baryon states classified within the $J = 1/2$ (left diagram) and $J = 3/2$ (right diagram) SU(3) $\mathbf{3}^*$ irreps. The question mark indicates states predicted in this work

Fig. 5 Charm and bottom resonances classified within SU(3) **6** irreps with $J = 1/2$, which however stem from different $\mathrm{SU(6)_{lsf}}\times$HQSS irreps: (**120**, **21**, $\mathbf{6_2}$) and (**168**, **15**, $\mathbf{6_2}$), respectively. The question mark indicates states predicted in this work

spin–parity. In our model we identify the $\Xi_b(6227)$ as a $1/2^-$ state and, again, the difference arises because of the renormalization scheme and the interaction matrices involving D, D^* and light vector mesons.

4 Conclusions

In this work we have explored the possible molecular interpretation of several experimental excited Ξ_c and Ξ_b states. We have used a coupled-channel unitarized model, that is based on a $\mathrm{SU(6)_{lsf}}\times$HQSS-extended WT baryon–meson interaction, within the on-shell approximation. We have paid a special attention to the dependence of our predictions on the renormalization scheme, so as to assess the robustness of our results.

We have presented a molecular interpretation for the experimental $\Xi_c(2790)$, $\Xi_c(2815)$, $\Xi_c(2930)$, $\Xi_c(2970)$ and $\Xi_b(6227)$ states, and have predicted the spin–parity quantum numbers of the latter three resonances. We have found that the $\Xi_c(2790)$ state has a large molecular $\Lambda_c\bar{K}$ component, with a dominant $j^{\pi}_{ldof} = 0^-$ configuration, and discussed the differences between the $3/2^-$ $\Lambda_c(2625)$ and $\Xi_c(2815)$ states, finding that they cannot be SU(3) siblings. We have also predicted the existence of other Ξ_c-states, not experimentally detected yet, being one of them related to the two-pole structure of the $\Lambda_c(2595)$. Interestingly, the recently discovered $\Xi_c(2930)$ and $\Xi_c(2970)$ are found to be HQSS partners.

The flavor-symmetry content of the framework has also allowed us to understand the nature of the $\Sigma_c(2800)$ and $\Sigma_b(6097)$ states, for which we have determined their spin–parity. Moreover, we have predicted several states, some of them displayed in Figs. 4 and 5 (marked with a ? symbol). Among them, we stress the $\Omega_b(6360)$ state, with a dominant $\Xi_b\bar{K}$ contribution, in the sextet where the $\Sigma_b(6097)$ and $\Xi_b(6227)$ are located, together with the $\Xi_b(6240)$ and $\Xi_b^*(6240)$ states, partners of the HQSS doublet $\Lambda_b(5912)$ and $\Lambda_b(5920)$ discussed in [24].

Acknowledgements L.T. acknowledges support from Deutsche Forschungsgemeinschaft under Project Nr. 383452331 (Heisenberg Programme) and Project Nr. 411563442. R. P. Pavao wishes to thank the Generalitat Valenciana in the program GRISOLIAP/2016/071. This research is supported by the Spanish Ministerio de Economía y Competitividad and the European Regional Development Fund, under contracts FIS2017-84038-C2-1-P, FPA2013-43425-P, FPA2016-81114-P and SEV-2014-0398; the THOR COST Action CA15213; and by the EU STRONG-2020 project under the program H2020-INFRAIA-2018-1, Grant agreement no. 824093.

Data Availability Statement This manuscript has no associated data or the data will not be deposited. [Authors' comment: The results of our work are already presented in the plots and tables of our paper, so there is no more data to be deposited elsewhere.]

Funded by SCOAP[3].

References

1. M. Tanabashi et al. (Particle Data Group). Phys. Rev. D **98**, 030001 (2018)
2. E. Klempt, J.-M. Richard, Rev. Mod. Phys. **82**, 1095 (2010). arXiv:0901.2055 [hep-ph]
3. V. Crede, W. Roberts, Rep. Prog. Phys. **76**, 076301 (2013). arXiv:1302.7299 [nucl-ex]
4. H.-Y. Cheng, Front. Phys. (Beijing) **10**, 101406 (2015)
5. H.-X. Chen, W. Chen, X. Liu, S.-L. Zhu, Phys. Rep. **639**, 1 (2016). arXiv:1601.02092 [hep-ph]
6. H.-X. Chen, W. Chen, X. Liu, Y.-R. Liu, S.-L. Zhu, Rep. Prog. Phys. **80**, 076201 (2017). arXiv:1609.08928 [hep-ph]

7. F.-K. Guo, C. Hanhart, U.-G. Meißner, Q. Wang, Q. Zhao, B.-S. Zou, Rev. Mod. Phys. **90**, 015004 (2018). arXiv:1705.00141 [hep-ph]
8. R. Aaij et al. (LHCb). Phys. Rev. Lett. **118**, 182001 (2017). arXiv:1703.04639 [hep-ex]
9. R. Aaij et al. (LHCb). Phys. Rev. Lett. **121**, 072002 (2018). arXiv:1805.09418 [hep-ex]
10. J. Yelton et al. (Belle). Phys. Rev. D **97**, 051102 (2018). arXiv:1711.07927 [hep-ex]
11. Y. Li et al. (Belle). Eur. Phys. J. C **78**, 252 (2018). arXiv:1712.03612 [hep-ex]
12. C.E. Jimenez-Tejero, A. Ramos, I. Vidana, Phys. Rev. C **80**, 055206 (2009). arXiv:0907.5316 [hep-ph]
13. J. Hofmann, M.F.M. Lutz, Nucl. Phys. A **763**, 90 (2005). arXiv:hep-ph/0507071 [hep-ph]
14. G. Montaña, A. Feijoo, A. Ramos, Eur. Phys. J. A **54**, 64 (2018). arXiv:1709.08737 [hep-ph]
15. V.R. Debastiani, J.M. Dias, W.H. Liang, E. Oset, Phys. Rev. D **97**, 094035 (2018). arXiv:1710.04231 [hep-ph]
16. C. Wang, L.-L. Liu, X.-W. Kang, X.-H. Guo, R.-W. Wang, Eur. Phys. J. C **78**, 407 (2018). arXiv:1710.10850 [hep-ph]
17. R. Chen, A. Hosaka, X. Liu, Phys. Rev. D **97**, 036016 (2018). arXiv:1711.07650 [hep-ph]
18. Q.X. Yu, R. Pavao, V.R. Debastiani, E. Oset, Eur. Phys. J. C **79**, 167 (2019). arXiv:1811.11738 [hep-ph]
19. J.-X. Lu, Y. Zhou, H.-X. Chen, J.-J. Xie, L.-S. Geng, Phys. Rev. D **92**, 014036 (2015). arXiv:1409.3133 [hep-ph]
20. Y. Huang, C.-J. Xiao, L.-S. Geng, J. He, Phys. Rev. D **99**, 014008 (2019). arXiv:1811.10769 [hep-ph]
21. C. Garcia-Recio et al., Phys. Rev. D **79**, 054004 (2009). arXiv:0807.2969 [hep-ph]
22. D. Gamermann, C. Garcia-Recio, J. Nieves, L.L. Salcedo, L. Tolos, Phys. Rev. D **81**, 094016 (2010). arXiv:1002.2763 [hep-ph]
23. O. Romanets, L. Tolos, C. Garcia-Recio, J. Nieves, L. Salcedo, R. Timmermans, Phys. Rev. D **85**, 114032 (2012). arXiv:1202.2239 [hep-ph]
24. C. Garcia-Recio, J. Nieves, O. Romanets, L. Salcedo, L. Tolos, Phys. Rev. D **87**, 034032 (2013a). arXiv:1210.4755 [hep-ph]
25. C. Garcia-Recio, J. Nieves, O. Romanets, L.L. Salcedo, L. Tolos, Phys. Rev. D **87**, 074034 (2013b). arXiv:1302.6938 [hep-ph]
26. L. Tolos, Int. J. Mod. Phys. E **22**, 1330027 (2013). arXiv:1309.7305 [nucl-th]
27. C. Garcia-Recio, C. Hidalgo-Duque, J. Nieves, L.L. Salcedo, L. Tolos, Phys. Rev. D **92**, 034011 (2015). arXiv:1506.04235 [hep-ph]
28. J. Nieves, R. Pavao, (2019), arXiv:1907.05747 [hep-ph]
29. J. Oller, U.G. Meissner, Phys. Lett. B **500**, 263 (2001)
30. D. Jido, J. Oller, E. Oset, A. Ramos, U. Meissner, Nucl. Phys. A **725**, 181 (2003)
31. T. Hyodo, W. Weise, Phys. Rev. C **77**, 035204 (2008). arXiv:0712.1613 [nucl-th]
32. R. Aaij et al. (LHCb). Phys. Rev. Lett. **109**, 172003 (2012). arXiv:1205.3452 [hep-ex]
33. J. Nieves, R. Pavao, L. Tolos, Eur. Phys. J. C **78**, 114 (2018). arXiv:1712.00327 [hep-ph]
34. J. Nieves, E. Ruiz Arriola, Phys. Rev. D **64**, 116008 (2001)
35. C. Garcia-Recio, J. Nieves, L.L. Salcedo, Phys. Rev. D **74**, 036004 (2006). arXiv:hep-ph/0605059 [hep-ph]
36. J. Hofmann, M.F.M. Lutz, Nucl. Phys. A **776**, 17 (2006). arXiv:hep-ph/0601249 [hep-ph]
37. C. Garcia-Recio, L. Geng, J. Nieves, L. Salcedo, Phys. Rev. D **83**, 016007 (2011). arXiv:1005.0956 [hep-ph]
38. F.-K. Guo, U.-G. Meißner, B.-S. Zou, Commun. Theor. Phys. **65**, 593 (2016). arXiv:1603.06316 [hep-ph]
39. M. Albaladejo, J. Nieves, E. Oset, Z.-F. Sun, X. Liu, Phys. Lett. B **757**, 515 (2016). arXiv:1603.09230 [hep-ph]
40. J. Yelton et al. (Belle). Phys. Rev. D **94**, 052011 (2016). arXiv:1607.07123 [hep-ex]
41. T. Yoshida, E. Hiyama, A. Hosaka, M. Oka, K. Sadato, Phys. Rev. D **92**, 114029 (2015). arXiv:1510.01067 [hep-ph]
42. C. Garcia-Recio, J. Nieves, E. Ruiz Arriola, M.J. Vicente Vacas, Phys. Rev. D **67**, 076009 (2003). arXiv:hep-ph/0210311d [hep-ph]
43. T. Hyodo, S. Nam, D. Jido, A. Hosaka, Phys. Rev. C **68**, 018201 (2003)
44. C. Garcia-Recio, M.F.M. Lutz, J. Nieves, Phys. Lett. B **582**, 49 (2004). arXiv:nucl-th/0305100 [nucl-th]
45. T. Hyodo, D. Jido, Prog. Part. Nucl. Phys. **67**, 55 (2012). arXiv:1104.4474 [nucl-th]
46. D. Gamermann, C. Garcia-Recio, J. Nieves, L. Salcedo, Phys. Rev. D **84**, 056017 (2011). arXiv:1104.2737 [hep-ph]
47. Y. Kamiya et al., Nucl. Phys. A **954**, 41 (2016). arXiv:1602.08852 [hep-ph]
48. R. Aaij et al. (LHCb). Phys. Rev. Lett. **122**, 012001 (2019). arXiv:1809.07752 [hep-ex]
49. W.-H. Liang, J.M. Dias, V.R. Debastiani, E. Oset, Nucl. Phys. B **930**, 524 (2018). arXiv:1711.10623 [hep-ph]